Different roles of myocardial ROCK1 and ROCK2 in cardiac dysfunction and postcapillary pulmonary hypertension in mice

Shinichiro Sunamura[a], Kimio Satoh[a], Ryo Kurosawa[a], Tomohiro Ohtsuki[a], Nobuhiro Kikuchi[a], Md. Elias-Al-Mamun[a], Toru Shimizu[a], Shohei Ikeda[a], Kota Suzuki[a], Taijyu Satoh[a], Junichi Omura[a], Masamichi Nogi[a], Kazuhiko Numano[a], Mohammad Abdul Hai Siddique[a], Satoshi Miyata[a], Masahito Miura[b], and Hiroaki Shimokawa[a,1]

[a]Department of Cardiovascular Medicine, Tohoku University Graduate School of Medicine, Sendai, Miyagi, 980-8574, Japan; and [b]Department of Clinical Physiology, Health Science, Tohoku University Graduate School of Medicine, Sendai, Miyagi, 980-8575, Japan

Edited by J. G. Seidman, Harvard Medical School, Boston, MA, and approved June 21, 2018 (received for review December 8, 2017)

Although postcapillary pulmonary hypertension (PH) is an important prognostic factor for patients with heart failure (HF), its pathogenesis remains to be fully elucidated. To elucidate the different roles of Rho-kinase isoforms, ROCK1 and ROCK2, in cardiomyocytes in response to chronic pressure overload, we performed transverse aortic constriction (TAC) in cardiac-specific ROCK1-deficient (*cROCK1*$^{-/-}$) and ROCK2-deficient (*cROCK2*$^{-/-}$) mice. Cardiomyocyte-specific ROCK1 deficiency promoted pressure-overload-induced cardiac dysfunction and postcapillary PH, whereas cardiomyocyte-specific ROCK2 deficiency showed opposite results. Histological analysis showed that pressure-overload-induced cardiac hypertrophy and fibrosis were enhanced in *cROCK1*$^{-/-}$ mice compared with controls, whereas cardiac hypertrophy was attenuated in *cROCK2*$^{-/-}$ mice after TAC. Consistently, the levels of oxidative stress were up-regulated in *cROCK1*$^{-/-}$ hearts and down-regulated in *cROCK2*$^{-/-}$ hearts compared with controls after TAC. Furthermore, cyclophilin A (CyPA) and basigin (Bsg), both of which augment oxidative stress, enhanced cardiac dysfunction and postcapillary PH in *cROCK1*$^{-/-}$ mice, whereas their expressions were significantly lower in *cROCK2*$^{-/-}$ mice. In clinical studies, plasma levels of CyPA were significantly increased in HF patients and were higher in patients with postcapillary PH compared with those without it. Finally, high-throughput screening demonstrated that celastrol, an antioxidant and antiinflammatory agent, reduced the expressions of CyPA and Bsg in the heart and the lung, ameliorating cardiac dysfunction and postcapillary PH induced by TAC. Thus, by differentially affecting CyPA and Bsg expressions, ROCK1 protects and ROCK2 jeopardizes the heart from pressure-overload HF with postcapillary PH, for which celastrol may be a promising agent.

heart failure | oxidative stress | Rho-kinase

Heart failure (HF) has been emerging as a pandemic health issue worldwide (1). HF patients are categorized into two groups by left ventricular ejection fraction (LVEF): HF with reduced LVEF (HFrEF) and HF with preserved LVEF (HFpEF) (2). Effective medical and surgical therapies for HFrEF are available, whereas no effective drugs are yet available for HFpEF (2, 3). This is partly due to our poor understanding of the pathogenesis of HFpEF, which is clinically characterized by cardiac hypertrophy, fibrosis, and diastolic dysfunction (4). Indeed, we have no option to reverse cardiac hypertrophy and fibrosis with medical treatment. Pressure overload, such as systemic hypertension and aortic valve stenosis (AS), causes cardiac hypertrophy and fibrosis, leading to HFpEF in early stages (5). Although cardiac hypertrophy is a primary response to reduce wall stress on the ventricular wall, sustained hypertrophic response eventually leads to cardiac dysfunction and failure (6). To date, the molecular mechanisms underlying cardiac hypertrophy and subsequent dysfunction and failure remain to be fully elucidated. Furthermore, severe HF is accompanied by postcapillary pulmonary hypertension (PH), which is characterized by impaired pulmonary vascular reactivity, endothelial dysfunction, and distal pulmonary artery muscularization (7, 8). Once postcapillary PH develops, HF patients show more severe symptoms, worse exercise tolerance, and poor prognosis (7, 9). Some possible treatments for postcapillary PH have been tested in animal models of HF (10, 11). While targeting both cardiac dysfunction and postcapillary PH could be a promising therapy for HF patients, therapeutic targets that share molecular mechanisms of both diseases need to be explored.

Rho-kinases (ROCKs), members of the serine/threonine protein kinase family, are important downstream effectors of the small GTP-binding protein Ras homolog gene family member A (RhoA) (12). The RhoA/Rho-kinase pathway plays important roles in many cellular functions, including contraction, motility, proliferation, and apoptosis (13). Thus, excessive activity of this pathway promotes the development of cardiovascular diseases (13), such as coronary vasospasm (14), hypertension (15), PH (16), and HF (17). Moreover, the beneficial effects of fasudil, a specific Rho-kinase inhibitor, have been demonstrated in those pathological conditions in both animal models and human studies (18–20). However, fasudil inhibits both isoforms of Rho-kinase, ROCK1 and ROCK2, which have different functions in different types of cells and tissues (21). In the field of HF, we and

Significance

Our data suggest opposite roles for ROCK1 and ROCK2 in cardiomyocytes. Additional studies identified downstream targets of ROCK1 and ROCK2 related to calcium handling, mitochondrial function, and oxidative stress. In particular, our findings indicate that cyclophilin A (CyPA) and basigin (Bsg), both of which augment oxidative stress, enhanced cardiac dysfunction and postcapillary pulmonary hypertension (PH) in *cROCK1*$^{-/-}$ mice, while their expressions were lower in *cROCK2*$^{-/-}$ mice. Finally, screening of the public chemical library in the Drug Discovery Initiative enabled us to identify compounds that reduce the expressions of CyPA and Bsg. Among them, celastrol suppressed the expression of both CyPA and Bsg in heart and lungs, thereby ameliorating both heart failure and postcapillary PH in mice.

Author contributions: S.S., K. Satoh, T. Shimizu, S.I., and H.S. designed research; S.S., R.K., T.O., N.K., M.E.-A.-M., K. Suzuki, T. Satoh, J.O., M.N., K.N., M.A.H.S., and M.M. performed research; S.S., S.M., and M.M. analyzed data; and S.S., K. Satoh, and H.S. wrote the paper.

The authors declare no conflict of interest.

This article is a PNAS Direct Submission.

[1]To whom correspondence should be addressed. Email: shimo@cardio.med.tohoku.ac.jp.

This article contains supporting information online at www.pnas.org/lookup/suppl/doi:10.1073/pnas.1721298115/-/DCSupplemental.

Published online July 9, 2018.

others previously demonstrated that ROCK2 plays a crucial role in cardiac hypertrophic responses (17, 22), while ROCK1 seems to be involved in cardiac fibrosis (23). However, the roles of each isoform in cardiomyocytes remain to be elucidated. In the present study, to elucidate the different roles of ROCK1 and ROCK2 in cardiomyocytes in response to chronic pressure overload, we performed transverse aortic constriction (TAC) in cardiac-specific ROCK1-deficient (*cROCK1*$^{-/-}$) and ROCK2-deficient (*cROCK2*$^{-/-}$) mice.

Results

Generation of *cROCK1*$^{-/-}$ and *cROCK2*$^{-/-}$ Mice. Cardiac troponins, which directly regulate myocardial contractility, are potential substrates of ROCK1 and ROCK2 (24). However, the specific substrates of each isotype and interactions between them in maintaining cardiac function have not been elucidated (25). Thus, to elucidate the different roles of ROCK1 and ROCK2 in cardiomyocytes in response to pressure overload, we generated cardiac-specific ROCK1-deficient (*ROCK1* $^{flox/flox}$/*aMHC-cre*$^{+/-}$; *cROCK1*$^{-/-}$) and ROCK2-deficient (*ROCK2* $^{flox/flox}$/*aMHC-cre*$^{+/-}$; *cROCK2*$^{-/-}$) mice (*SI Appendix*, Fig. S1 *A* and *B*). We first compared cardiac structure and function between *cROCK1*$^{+/+}$ (*ROCK1* $^{flox/flox}$/*aMHC-cre*$^{-/-}$), *cROCK2*$^{+/+}$ (*ROCK2* $^{flox/flox}$/*aMHC-cre*$^{-/-}$), and *aMHC-cre*$^{+/-}$ mice at baseline by echocardiographic examination. As we found no significant difference in left ventricular (LV) posterior wall thickness (LVPW), LV internal diameter at end-diastole (LVDd), or LV fractional shortening (LVFS) among them, we used *cROCK1*$^{+/+}$ and *cROCK2*$^{+/+}$ mice as littermate controls (*SI Appendix*, Fig. S1*C*). We next examined the expression levels of ROCK1 and ROCK2 by immunofluorescence staining and found that ROCK1 and ROCK2 expressions were deleted in ∼95% of total cells in the adult hearts (*SI Appendix*, Fig. S1*D*). *cROCK1*$^{+/+}$ and *cROCK1*$^{-/-}$ mice and *cROCK2*$^{+/+}$ and *cROCK2*$^{-/-}$ mice showed normal growth under physiological conditions. At baseline, there was no difference in blood pressure or heart rate between *cROCK1*$^{+/+}$ and *cROCK1*$^{-/-}$ mice (*SI Appendix*, Fig. S2*A*) and between *cROCK2*$^{+/+}$ and *cROCK2*$^{-/-}$ mice (*SI Appendix*, Fig. S2*B*). We next performed microarray analyses to examine the difference in gene expression in cardiac tissues between *cROCK1*$^{-/-}$ and *cROCK2*$^{-/-}$ mice at baseline. Genes with significant changes were submitted to Ingenuity Pathway Analysis (IPA) software to reveal gene sets representing specific biological processes or functions. Interestingly, heat-map analysis showed that the gene sets from *cROCK1*$^{-/-}$ hearts showed up-regulations of the pathways related to cardiac hypertrophy, fibrosis, and HF compared with *cROCK1*$^{+/+}$ hearts (*SI Appendix*, Fig. S2*C*), whereas *cROCK2*$^{-/-}$ hearts showed down-regulations of these signaling pathways compared with *cROCK2*$^{+/+}$ hearts (*SI Appendix*, Fig. S2*D*). For example, the IPA analysis showed significant alteration in RhoA signaling in *cROCK1*$^{-/-}$ hearts (*SI Appendix*, Table S1), whereas in *cROCK2*$^{-/-}$ hearts, RhoA signaling was not involved in the top 10 significant changes in the canonical pathways (*SI Appendix*, Table S2). Moreover, *cROCK1*$^{-/-}$ hearts showed significant alteration in calcium handling signaling compared with *cROCK1*$^{+/+}$ hearts (*SI Appendix*, Table S1), whereas *cROCK2*$^{-/-}$ hearts presented significant alteration in cardiac β-adrenergic signaling compared with *cROCK2*$^{+/+}$ hearts (*SI Appendix*, Table S2). These results indicate that ROCK1 and ROCK2 possess completely different and potentially contrasting roles in cardiomyocytes.

Crucial Roles of ROCK1 in Cardiomyocytes to Maintain Systolic Function. Although several ROCK1-specific substrates have been reported (26), the role of ROCK1 in cardiomyocytes remains to be fully elucidated. Thus, to examine the role of ROCK1 in cardiomyocytes under pressure overload we performed TAC in *cROCK1*$^{+/+}$ and *cROCK1*$^{-/-}$ mice. Echocardiographic examination showed that TAC progressively induced cardiac hypertrophy in both genotypes as examined by LVPW, the extent of which was comparable between *cROCK1*$^{+/+}$ and *cROCK1*$^{-/-}$ mice (Fig. 1 *A* and *B* and *SI Appendix*, Fig. S3*A*). TAC also progressively increased LVDd in both genotypes, the extent of which was greater

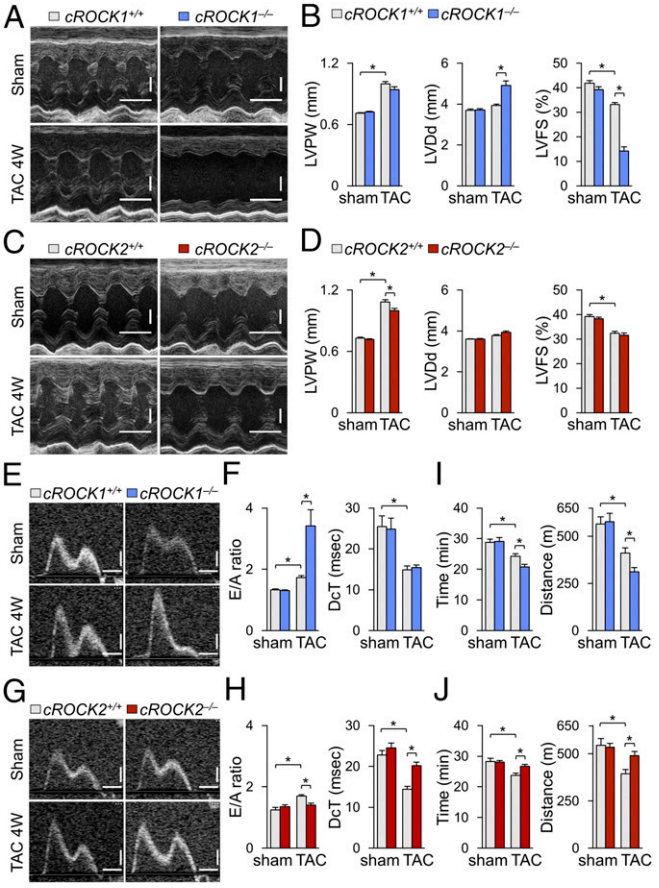

Fig. 1. Different roles of ROCK1 and ROCK2 in response to pressure overload. (*A*) Representative echocardiographic M-mode images of left ventricles in *cROCK1*$^{+/+}$ and *cROCK1*$^{-/-}$ mice 4 wk after TAC or sham operation. (Scale bars, 100 ms and 1 mm.) (*B*) Quantitative analysis of the parameters of cardiac function in *cROCK1*$^{+/+}$ and *cROCK1*$^{-/-}$ mice at 4 wk after TAC (n = 12 each) or sham operation (n = 5 each). (*C*) Representative echocardiographic M-mode images of left ventricles in *cROCK2*$^{+/+}$ and *cROCK2*$^{-/-}$ mice 4 wk after TAC or sham operation. (Scale bars, 100 ms and 1 mm.) (*D*) Quantitative analysis of the parameters of cardiac function in *cROCK2*$^{+/+}$ and *cROCK2*$^{-/-}$ mice at 4 wk after TAC (n = 12 each) or sham operation (n = 5 each). (*E*) Representative echocardiographic images of mitral inflow pattern to evaluate diastolic dysfunction in *cROCK1*$^{+/+}$ and *cROCK1*$^{-/-}$ mice 4 wk after TAC or sham operation. (Scale bars, 20 ms and 200 mm/s.) (*F*) Quantitative analysis of the parameters of diastolic function measured by transmitral Doppler velocity ratio of early-to-atrial wave (E/A ratio) and early wave decelation time (DcT) in *cROCK1*$^{+/+}$ and *cROCK1*$^{-/-}$ mice at 4 wk after TAC (n = 12 each) or sham operation (n = 5 each). (*G*) Representative echocardiographic images of mitral inflow pattern to evaluate diastolic dysfunction in *cROCK2*$^{+/+}$ and *cROCK2*$^{-/-}$ mice 4 wk after TAC or sham operation. (Scale bars, 20 ms and 200 mm/s.) (*H*) Quantitative analysis of the parameters of diastolic function measured by E/A ratio and DcT in *cROCK2*$^{+/+}$ and *cROCK2*$^{-/-}$ mice at 4 wk after TAC (n = 12 each) or sham operation (n = 5 each). (*I*) Exercise tolerance evaluated by measuring running time and distance in a treadmill running test in *cROCK1*$^{+/+}$ and *cROCK1*$^{-/-}$ mice at 4 wk after TAC (n = 12 each) or sham operation (n = 5 each). (*J*) Exercise tolerance evaluated by measuring walking time and distance in a treadmill test in *cROCK2*$^{+/+}$ and *cROCK2*$^{-/-}$ mice at 4 wk after TAC (n = 12 each) or sham operation (n = 5 each). Data represent the mean ± SEM; *P < 0.05. Comparisons of parameters were performed with two-way ANOVA, followed by Tukey's honestly significant difference test for multiple comparisons.

in *cROCK1*$^{-/-}$ mice than in *cROCK1*$^{+/+}$ mice (Fig. 1*B* and *SI Appendix*, Fig. S3*B*). Consistently, TAC significantly reduced LVFS in both genotypes in a time-dependent manner, the extent of which was greater in *cROCK1*$^{-/-}$ mice than in *cROCK1*$^{+/+}$ mice (Fig. 1*B* and *SI Appendix*, Fig. S3*C*). Next, to examine the role of ROCK2 in cardiomyocytes under pressure overload, we performed TAC in *cROCK2*$^{+/+}$ and *cROCK2*$^{-/-}$ mice. Echocardiographic examination showed that TAC induced cardiac hypertrophy in both genotypes as examined by LVPW and the extent of the hypertrophy was significantly smaller in *cROCK2*$^{-/-}$ mice than in *cROCK2*$^{+/+}$ mice (Fig. 1 *C* and *D*). In contrast to *cROCK1*$^{-/-}$ mice, there was no difference in LVDd or LVFS between *cROCK2*$^{+/+}$ and *cROCK2*$^{-/-}$ mice (Fig. 1 *C* and *D*). These results indicate that myocardial ROCK1 plays a crucial role to maintain systolic function under pressure overload, whereas myocardial ROCK2 plays a crucial role in the development of cardiac hypertrophy under pressure overload.

ROCK2 in Cardiomyocytes Induces Diastolic Dysfunction Under Pressure Overload. To evaluate the role of ROCK1 in the development of diastolic dysfunction, we examined transmitral Doppler flow velocity after TAC. TAC increased E/A velocity ratio in both genotypes, the extent of which was significantly greater in *cROCK1*$^{-/-}$ mice than in *cROCK1*$^{+/+}$ mice, suggesting that diastolic dysfunction is exacerbated by ROCK1 deficiency (Fig. 1 *E* and *F* and *SI Appendix*, Fig. S3*D*). Next, we examined the development of diastolic dysfunction in *cROCK2*$^{-/-}$ mice in response to pressure overload. TAC increased E/A velocity ratio in *cROCK2*$^{+/+}$ mice, whereas the ratio was significantly smaller in *cROCK2*$^{-/-}$ mice (Fig. 1 *G* and *H*). Additionally, transmitral Doppler flow velocity showed slower deceleration of the mitral E wave (longer DcT) in *cROCK2*$^{-/-}$ mice than in *cROCK2*$^{+/+}$ mice, suggesting that the development of diastolic dysfunction is attenuated by ROCK2 deficiency (Fig. 1 *G* and *H*). Moreover, to evaluate the filling pressure after pressure overload, we examined atrial size and E/e′ after TAC by echocardiography. TAC significantly increased both atrial size and E/e′, the extent of which was greater in *cROCK1*$^{-/-}$ mice but smaller in *cROCK2*$^{-/-}$ mice compared with their respective controls (*SI Appendix*, Fig. S4 *A* and *B*). Time-course analysis also revealed that atrial size and E/e′ were increased in *cROCK1*$^{-/-}$ mice earlier after TAC compared with *cROCK1*$^{+/+}$ mice (*SI Appendix*, Fig. S3 *E* and *F*). Consistently, catheter examination showed that TAC significantly elevated LV end-diastolic pressure compared with sham controls, the extent of which was greater in *cROCK1*$^{-/-}$ mice but smaller in *cROCK2*$^{-/-}$ mice compared with their respective controls (*SI Appendix*, Fig. S4 *C* and *D*). These results indicate that elevated filling pressures caused by pressure overload are enhanced by ROCK1 deficiency but are attenuated by ROCK2 deficiency. To further assess the exercise capacity after pressure overload, we performed a treadmill test and examined the walking distance and time. At baseline, there was no difference in exercise capacity between *cROCK1*$^{+/+}$ and *cROCK1*$^{-/-}$ mice (Fig. 1*I*), whereas pressure overload significantly reduced the walking distance and time in both genotypes. However, walking distance and time were significantly more reduced in *cROCK1*$^{-/-}$ mice than in *cROCK1*$^{+/+}$ mice (Fig. 1*I*). Likewise, we performed a treadmill test in *cROCK2*$^{+/+}$ and *cROCK2*$^{-/-}$ mice. Again, TAC reduced the walking distance and time in *cROCK2*$^{+/+}$ mice, whereas exercise capacity was preserved in *cROCK2*$^{-/-}$ mice under pressure overload (Fig. 1*J*). Overall, ROCK1 in cardiomyocytes protects against the development of diastolic dysfunction and preserves the exercise capacity under pressure overload, whereas ROCK2 in cardiomyocytes promotes the development of diastolic dysfunction and reduces the exercise capacity under pressure overload.

Expression of ROCK1 and ROCK2 in Cardiomyocytes Under Pressure Overload. We next performed Western blotting to examine the expression levels of ROCK1, ROCK2, and upstream RhoA in the heart of each genotype under pressure overload. Pressure overload tended to increase ROCK1 expression compared with sham, which was significantly lower in *cROCK1*$^{-/-}$ hearts than in *cROCK1*$^{+/+}$ hearts (*SI Appendix*, Fig. S5*A*). Interestingly, ROCK2 was significantly up-regulated in *cROCK1*$^{-/-}$ hearts compared with *cROCK1*$^{+/+}$ hearts, especially under pressure overload (*SI Appendix*, Fig. S5*A*). Similarly, RhoA was significantly up-regulated in *cROCK1*$^{-/-}$ hearts compared with *cROCK1*$^{+/+}$ hearts at baseline and under pressure overload (*SI Appendix*, Fig. S5*A*). These results suggest that ROCK1 deficiency in cardiomyocytes up-regulates RhoA/ROCK2 signaling, probably due to compensatory mechanisms. Pressure overload tended to increase ROCK1 expression in *cROCK2*$^{+/+}$ and *cROCK2*$^{-/-}$ hearts to a similar level compared with sham (*SI Appendix*, Fig. S5*B*). Additionally, TAC-induced up-regulation of ROCK2 in *cROCK2*$^{+/+}$ and *cROCK2*$^{-/-}$ hearts was significantly lower in *cROCK2*$^{-/-}$ hearts than in *cROCK2*$^{+/+}$ hearts (*SI Appendix*, Fig. S5*B*). Moreover, RhoA was significantly up-regulated in *cROCK2*$^{-/-}$ hearts compared with *cROCK2*$^{+/+}$ hearts only under pressure overload (*SI Appendix*, Fig. S5*B*). These results suggest that ROCK2 deficiency up-regulates RhoA under pressure overload. However, ROCK2 deficiency in cardiomyocytes did not affect ROCK1 expression both at baseline and under pressure overload, showing clear differences from ROCK1 deficiency.

Next, we examined the localization of ROCK1 and ROCK2 expressions in the heart in each genotype by immunofluorescence staining. As expected, ROCK1 expression was absent in *cROCK1*$^{-/-}$ cardiomyocytes, while ROCK1 expression was detected in noncardiomyocytes (e.g., cardiac fibroblasts and migrating inflammatory cells) that contributed to ROCK1 detection in Western blots (*SI Appendix*, Fig. S5*C*). Indeed, double immunostaining showed that ROCK1 was also strongly expressed in perivascular periostin-positive cells and CD45-positive cells (*SI Appendix*, Fig. S6 *A* and *B*). Likewise, ROCK2 expression was absent in *cROCK2*$^{-/-}$ cardiomyocytes, whereas ROCK2 expression was detected in noncardiomyocytes that contributed to ROCK2 detection in Western blots (*SI Appendix*, Fig. S5*D*). Indeed, double immunostaining showed that ROCK2 was also strongly expressed in perivascular periostin-positive cells and CD45-positive cells (*SI Appendix*, Fig. S6 *C* and *D*).

Opposite Roles of ROCK1 and ROCK2 in Cardiomyocytes. The analyses of induction and interaction of ROCK isoforms in cardiomyocytes indicated different roles of ROCK1 and ROCK2 in cardiac responses to pressure overload. Indeed, pressure overload significantly enhanced cardiac hypertrophy, assessed by the ratio of heart weight/body weight, in both *cROCK1*$^{+/+}$ and *cROCK1*$^{-/-}$ mice, but the extent was significantly greater in *cROCK1*$^{-/-}$ mice than in *cROCK1*$^{+/+}$ mice (Fig. 2*A*). Consistently, pressure overload significantly increased cross-sectional area (CSA) in *cROCK1*$^{-/-}$ hearts compared with *cROCK1*$^{+/+}$ hearts (Fig. 2*B*). Likewise, pressure overload significantly increased cardiac hypertrophy in *cROCK2*$^{+/+}$ mice (Fig. 2*C*). However, the extent of hypertrophic response was significantly smaller in *cROCK2*$^{-/-}$ mice than in *cROCK2*$^{+/+}$ mice (Fig. 2*C*). Consistently, TAC-induced increase in CSA was significantly smaller in *cROCK2*$^{-/-}$ hearts than in *cROCK2*$^{+/+}$ hearts (Fig. 2*D*). Consistent with the histological analyses, the expressions of genes encoding hypertrophic markers (e.g., *Nppa* and *Nppb*) were significantly up-regulated in *cROCK1*$^{-/-}$ hearts compared with *cROCK1*$^{+/+}$ hearts, especially under pressure overload (Fig. 2*E*). In contrast, hypertrophic gene expression was significantly lower in *cROCK2*$^{-/-}$ hearts than in *cROCK2*$^{+/+}$ hearts under pressure overload (Fig. 2*F*). These results indicate that ROCK1 protects against the development of cardiac hypertrophy and

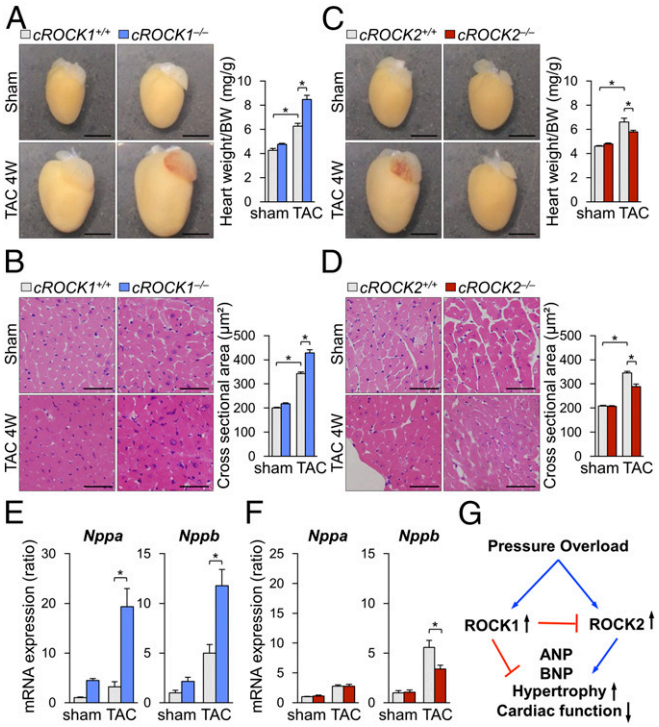

Fig. 2. Opposite roles of ROCK1 and ROCK2 in cardiac hypertrophy. (*A*, *Left*) Representative photomicrographs of hearts from *cROCK1*$^{+/+}$ and *cROCK1*$^{-/-}$ mice 4 wk after TAC or sham operation. (*A*, *Right*) The ratio of heart weight to body weight (BW) in *cROCK1*$^{+/+}$ and *cROCK1*$^{-/-}$ mice at 4 wk after TAC (n = 12 each) or sham operation (n = 5 each). (Scale bars, 3 mm.) (*B*, *Left*) Representative photomicrographs of H&E staining of hearts from *cROCK1*$^{+/+}$ and *cROCK1*$^{-/-}$ mice 4 wk after TAC or sham operation. (*B*, *Right*) Quantitative analysis of cardiomyocyte CSA in *cROCK1*$^{+/+}$ and *cROCK1*$^{-/-}$ mice at 4 wk after TAC (n = 10 each) or sham operation (n = 5 each). (Scale bars, 50 μm.) (*C*, *Left*) Representative photomicrographs of hearts from *cROCK2*$^{+/+}$ and *cROCK2*$^{-/-}$ mice 4 wk after TAC or sham operation. (*C*, *Right*) The ratio of heart weight to body weight (BW) in *cROCK2*$^{-/-}$ and *cROCK2*$^{+/+}$ mice at 4 wk after TAC (n = 12 each) or sham operation (n = 5 each). (Scale bars, 3 mm.) (*D*, *Left*) Representative photomicrographs of H&E staining of hearts from *cROCK2*$^{+/+}$ and *cROCK2*$^{-/-}$ mice 4 wk after TAC or sham operation. (*D*, *Right*) Quantitative analysis of cardiomyocyte CSA in *cROCK2*$^{-/-}$ and *cROCK2*$^{+/+}$ mice at 4 wk after TAC (n = 10 each) or sham operation (n = 5 each). (Scale bars, 50 μm.) (*E*) Relative mRNA expressions of hypertrophic markers, such as natriuretic peptide A (*Nppa*) and natriuretic peptide B (*Nppb*), in *cROCK1*$^{+/+}$ and *cROCK1*$^{-/-}$ hearts at 4 wk after TAC (n = 12 each) or sham operation (n = 5 each). (*F*) Relative mRNA expressions of hypertrophic markers in *cROCK2*$^{+/+}$ and *cROCK2*$^{-/-}$ hearts at 4 wk after TAC (n = 12 each) or sham operation (n = 5 each). (*G*) Schematic representation of the opposite roles of ROCK1 and ROCK2 in the development of pressure-overload-induced cardiac hypertrophy. *P < 0.05. Comparisons of parameters were performed with two-way ANOVA, followed by Tukey's honestly significant difference test for multiple comparisons.

dysfunction under pressure overload, whereas ROCK2 plays opposite roles in cardiomyocytes (Fig. 2*G*).

In addition to the hypertrophic responses, Elastica-Masson (EM) staining showed that TAC significantly increased the interstitial fibrosis area in *cROCK1*$^{+/+}$ and *cROCK1*$^{-/-}$ hearts (*SI Appendix*, Fig. S7*A*), but the extent was significantly greater in *cROCK1*$^{-/-}$ hearts than in *cROCK1*$^{+/+}$ hearts under pressure overload (*SI Appendix*, Fig. S7*A*). Consistently, gene expressions of fibrotic markers (e.g., *Col1a* and *Col3a*) were significantly upregulated in *cROCK1*$^{-/-}$ hearts compared with *cROCK1*$^{+/+}$ hearts under pressure overload (*SI Appendix*, Fig. S7*B*). Likewise, pressure overload significantly increased the interstitial fibrosis area in *cROCK2*$^{+/+}$ and *cROCK2*$^{-/-}$ hearts (*SI Appendix*, Fig. S7*C*). However, the extent of the increase was comparable between *cROCK2*$^{+/+}$ and *cROCK2*$^{-/-}$ hearts (*SI Appendix*, Fig. S7*C*). Consistently, gene expressions of fibrotic markers were comparable between *cROCK2*$^{+/+}$ and *cROCK2*$^{-/-}$ hearts (*SI Appendix*, Fig. S7*D*). Based on the different role of ROCK isoforms in interstitial fibrosis, we further examined matrix metalloproteinase (MMP) activities, assessed by DQ gelatin, in each genotype. Staining with DQ gelatin, in which green fluorescence indicates active MMPs, showed that TAC-induced MMP activities were significantly greater in *cROCK1*$^{-/-}$ hearts than in *cROCK1*$^{+/+}$ hearts (*SI Appendix*, Fig. S7*E*). However, the activities were significantly smaller in *cROCK2*$^{-/-}$ hearts than in *cROCK2*$^{+/+}$ hearts under pressure overload (*SI Appendix*, Fig. S7*F*). These results indicate that ROCK1 protects against the development of cardiac fibrosis and extracellular remodeling under pressure overload, while ROCK2 in cardiomyocytes does not play major roles in fibrosis (*SI Appendix*, Fig. S7*G*).

Opposite Roles of ROCK1 and ROCK2 in Cardiomyocytes for Ca^{2+} Handling. Intracellular Ca^{2+} handling and β-adrenergic stimulus are important for the development of cardiac hypertrophy and fibrosis under pressure overload (27). In the present study, microarray analysis indicated alterations in Ca^{2+} handling in *cROCK1*$^{-/-}$ hearts (*SI Appendix*, Table S1) and β-adrenergic signaling in *cROCK2*$^{-/-}$ hearts (*SI Appendix*, Table S2). Thus, we further analyzed the different roles of ROCK1 and ROCK2 in the regulation of Ca^{2+} handling in cardiomyocytes. Interestingly, pressure overload significantly reduced the phosphorylation of troponin I (TnI), which reduces calcium sensitivity in cardiomyocytes in both *cROCK1*$^{+/+}$ and *cROCK1*$^{-/-}$ hearts, but the extent of the reduction was significantly greater in *cROCK1*$^{-/-}$ hearts than in *cROCK1*$^{+/+}$ hearts (*SI Appendix*, Fig. S8*A*). Likewise, pressure overload significantly reduced TnI phosphorylation in both *cROCK2*$^{+/+}$ and *cROCK2*$^{-/-}$ hearts, but the extent of the reduction was comparable (*SI Appendix*, Fig. S8*B*). Additionally, TAC reduced phosphorylation of phospholamban (PLN), which activates Ca^{2+} pump in the sarcoplasmic reticulum equally in *cROCK1*$^{+/+}$ and *cROCK1*$^{-/-}$ hearts (*SI Appendix*, Fig. S8*A*). In contrast, the levels of PLN phosphorylation (S16 and T17) were significantly higher in *cROCK2*$^{-/-}$ hearts than in *cROCK2*$^{+/+}$ hearts both at baseline and under pressure overload (*SI Appendix*, Fig. S8*B*).

To elucidate the underlying molecular mechanism, we next examined the expression levels of genes related to Ca^{2+} handling. Gene expression of *Atp2a2*, one of the SERCA Ca^{2+}-ATPases, was down-regulated in *cROCK1*$^{-/-}$ hearts compared with the controls both at baseline and under pressure overload (*SI Appendix*, Fig. S8*C*). Additionally, pressure overload significantly increased *Pln* expression in both *cROCK1*$^{+/+}$ and *cROCK2*$^{+/+}$ hearts, which was significantly lower in *cROCK1*$^{-/-}$ and *cROCK2*$^{-/-}$ hearts than in the respective controls under pressure overload (*SI Appendix*, Fig. S8 *C* and *D*). Moreover, *cROCK1*$^{-/-}$ hearts showed significantly higher gene expression of *Ryr2*, which induces calcium-induced calcium release, compared with *cROCK1*$^{+/+}$ hearts at baseline, whereas the levels were down-regulated under pressure overload (*SI Appendix*, Fig. S8*C*). In contrast, *cROCK2*$^{-/-}$ hearts showed comparable gene expression of *Ryr2* compared with *cROCK2*$^{+/+}$ hearts at baseline, whereas the levels were significantly down-regulated under pressure overload (*SI Appendix*, Fig. S8*D*). Finally, pressure overload significantly increased the expression of *Slc8a1*, which encodes Na^{+}/Ca^{2+} exchanger, in both *cROCK1*$^{+/+}$ and *cROCK2*$^{+/+}$ hearts, but the extent was significantly smaller in *cROCK2*$^{-/-}$ hearts than in *cROCK1*$^{-/-}$ hearts under pressure overload (*SI Appendix*, Fig. S8 *C* and *D*). These results indicate that ROCK1 and ROCK2 play different roles in Ca^{2+} handling in cardiomyocytes, potentially leading to opposite roles of each isotype in the development of cardiac hypertrophy, fibrosis, and dysfunction under pressure overload (*SI Appendix*, Fig. S8*E*).

Based on the different roles of ROCK1 and ROCK2 in Ca^{2+} handling in cardiomyocytes, we performed additional experiments using the trabeculae from *cROCK1*$^{-/-}$ and *cROCK2*$^{-/-}$ hearts. We examined the force and intracellular Ca^{2+} concentration, $[Ca^{2+}]_i$, in the trabeculae during electrical stimulation (28). There was no difference in the force and $[Ca^{2+}]_i$ between the trabeculae from *cROCK1*$^{+/+}$ and *cROCK1*$^{-/-}$ hearts at low $[Ca^{2+}]_o$ (*SI Appendix*, Fig. S9 *A* and *B*). In contrast, at higher $[Ca^{2+}]_o$, the force and $[Ca^{2+}]_i$ of *cROCK1*$^{+/+}$ trabeculae increased in a $[Ca^{2+}]_o$-dependent manner, whereas the *cROCK1*$^{-/-}$ trabeculae did not respond (*SI Appendix*, Fig. S9 *A* and *B*). Again, the force and $[Ca^{2+}]_i$ of the trabeculae from *cROCK2*$^{+/+}$ and *cROCK2*$^{-/-}$ hearts increased in a $[Ca^{2+}]_o$-dependent manner (*SI Appendix*, Fig. S9 *C* and *D*).

Conflicting Roles of ROCK1 and ROCK2 in Cardiomyocytes for Reactive Oxygen Species Induction. To further elucidate the roles of ROCK1 and ROCK2, we used neonatal rat cardiomyocytes (NRCMs), which were stimulated with cyclic mechanical stretch (1 Hz, 20% elongation) (29). Cyclic mechanical stretch significantly increased the expression of ROCK1 and ROCK2 in NRCMs in a time-dependent manner (Fig. 3*A*). Consistently, Rho-kinase activity, assessed by phosphorylation of myosin phosphatase targeting protein (MYPT), was significantly increased in response to cyclic mechanical stretch in a time-dependent manner (Fig. 3*A*). Next, to evaluate the regulation of ROCK2 by ROCK1, we used siRNA to inhibit ROCK1 in NRCMs (Fig. 3*B*). Consistent with the ROCK2 up-regulation in *cROCK1*$^{-/-}$ hearts, ROCK1 inhibition in NRCMs significantly increased ROCK2 expression, whereas ROCK2 inhibition did not affect ROCK1 expression (Fig. 3*B*). These results indicate that mechanical stretch up-regulates both ROCK1 and ROCK2 in cardiomyocytes and that ROCK1 in cardiomyocytes down-regulates ROCK2 expression by unknown mechanism. Thus, to understand the mechanism underlying the regulation of ROCK1 and ROCK2 in cardiomyocytes, we examined the expressions of NOX2, NOX4, and p47^{phox} after inhibition of ROCK1 and ROCK2 in NRCMs (Fig. 3*C*). Interestingly, ROCK1 silencing by siRNA significantly increased the expressions of *Cybb* (NOX2), *Nox4*, and *Ncf1* (p47^{phox}) (Fig. 3*C*), while ROCK2 silencing reduced the expression of *Cybb* and *Ncf1* (Fig. 3*C*). These results suggest that ROCK1 and ROCK2 have opposite roles in the production of reactive oxygen species (ROS). Thus, we examined the levels of ROS in *cROCK1*$^{-/-}$ and *cROCK2*$^{-/-}$ hearts under pressure overload. Dihydroethidium (DHE) staining showed that pressure overload significantly increased ROS in *cROCK1*$^{-/-}$ hearts compared with *cROCK1*$^{+/+}$ hearts, whereas *cROCK2*$^{-/-}$ hearts presented lower ROS levels than *cROCK2*$^{+/+}$ hearts (Fig. 3*D*). We thus examined the expressions of *Cybb*, *Nox4*, and *Ncf1* in *cROCK1*$^{-/-}$ and *cROCK2*$^{-/-}$ hearts by quantitative real-time PCR. Notably, the expressions of *Cybb*, *Nox4*, and *Ncf1* were significantly increased in *cROCK1*$^{-/-}$ hearts compared with *cROCK1*$^{+/+}$ hearts under pressure overload (Fig. 3*E*). In contrast, *Nox4* expression was significantly lower in *cROCK2*$^{-/-}$ hearts than in *cROCK2*$^{+/+}$ hearts under pressure overload (Fig. 3*F*). These data indicate that ROCK1 inhibits ROS production in cardiomyocytes under pressure overload, whereas ROCK2 promotes it (Fig. 3*G*).

Conflicting Roles of ROCK1 and ROCK2 in Mitochondrial Function. Mitochondrial ROS levels regulate mitochondrial function and activities, which affects ATP production as an energy source in cardiomyocytes (30). Thus, we next examined the levels of mitochondrial ROS in *cROCK1*$^{-/-}$ and *cROCK2*$^{-/-}$ hearts under pressure overload. MitoSOX staining showed that mitochondrial ROS levels were higher in *cROCK1*$^{-/-}$ hearts than in *cROCK1*$^{+/+}$ hearts, whereas *cROCK2*$^{-/-}$ hearts presented lower levels of mitochondrial ROS than *cROCK2*$^{+/+}$ hearts (Fig. 4*A*). We thus

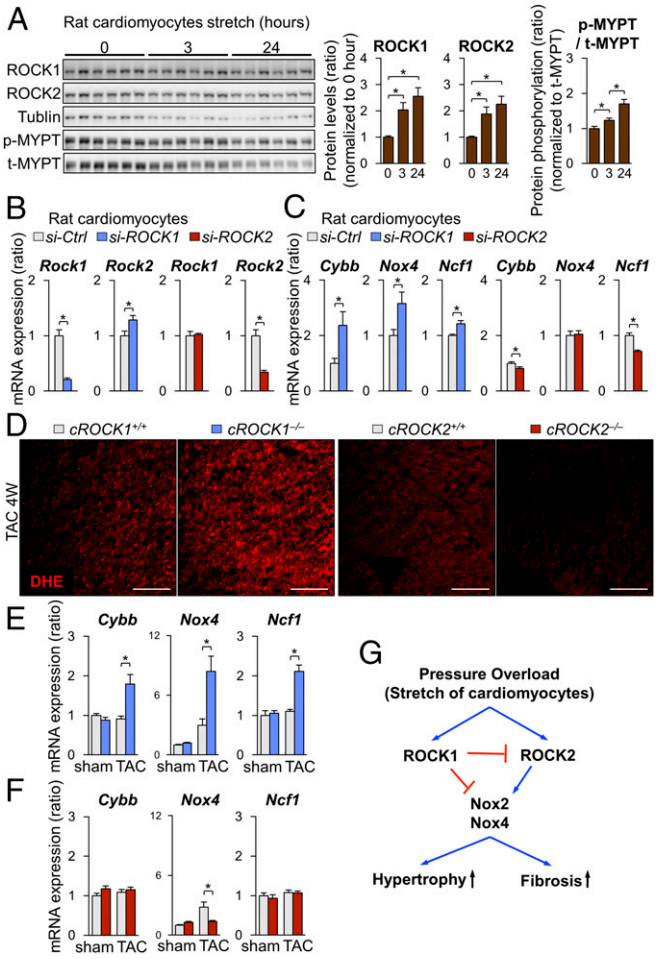

Fig. 3. Conflicting roles of ROCK1 and ROCK2 in cardiomyocytes for ROS induction. (*A*) Representative Western blot and quantification of ROCK1, ROCK2, and phosphorylated/total MYPT in NRCMs after mechanical cyclic stretch (1 Hz, 20% elongation) for 0, 3, and 24 h ($n = 6$ each). (*B*) Relative mRNA expression of *Rock1* and *Rock2* in NRCMs after transfection with ROCK1 siRNA (*si-ROCK1*), ROCK2 siRNA (*si-ROCK2*), or control siRNA (*si-Ctrl*) ($n = 4$ each). (*C*) Relative mRNA expressions of *Cybb* (NOX2), *Nox4*, and *Ncf1* (p47^{phox}) in NRCMs after transfection with *si-ROCK1*, *si-ROCK2*, or *si-Ctrl* ($n = 4$ each). (*D*) Representative pictures of DHE staining of the LV after TAC. (Scale bars, 100 μm.) (*E*) Relative mRNA expression of *Cybb* (NOX2), *Nox4*, and *Ncf1* (p47^{phox}), in *cROCK1*$^{+/+}$ and *cROCK1*$^{-/-}$ hearts at 4 wk after TAC ($n = 12$ each) or sham operation ($n = 5$ each). (*F*) Relative mRNA expression of *Cybb*, *Nox4*, and *Ncf1*, in *cROCK2*$^{+/+}$ and *cROCK2*$^{-/-}$ hearts at 4 wk after TAC ($n = 12$ each) or sham operation ($n = 5$ each). (*G*) Schematic representation of opposing roles of ROCK1 and ROCK2 in cardiomyocytes for ROS production. Data represent the mean ± SEM; $*P < 0.05$. Comparisons of parameters were performed with the unpaired Student's *t* test or two-way ANOVA followed by Tukey's honestly significant difference test for multiple comparisons.

examined the expressions of *Ppargc1a*, *Tfam*, *Cytb*, and *Nd5/6*, all of which regulate mitochondrial biogenesis, in *cROCK1*$^{-/-}$ and *cROCK2*$^{-/-}$ hearts by quantitative real-time PCR. Notably, *Ppargc1a* expression was significantly lower in *cROCK1*$^{-/-}$ hearts than in *cROCK1*$^{+/+}$ hearts under pressure overload (*SI Appendix*, Fig. S10*A*). In contrast, the expressions of *Tfam*, *Cytb*, and *Nd5/6* were higher in *cROCK1*$^{-/-}$ hearts than in *cROCK1*$^{+/+}$ hearts under pressure overload (*SI Appendix*, Fig. S10*A*). In contrast, *Ppargc1a*, *Cytb*, and *Nd5/6* expression did not significantly change in *cROCK2*$^{-/-}$ hearts compared with *cROCK2*$^{+/+}$ hearts under pressure overload (*SI Appendix*, Fig. S10*B*). We next examined the expressions of genes associated with mitochondrial fission

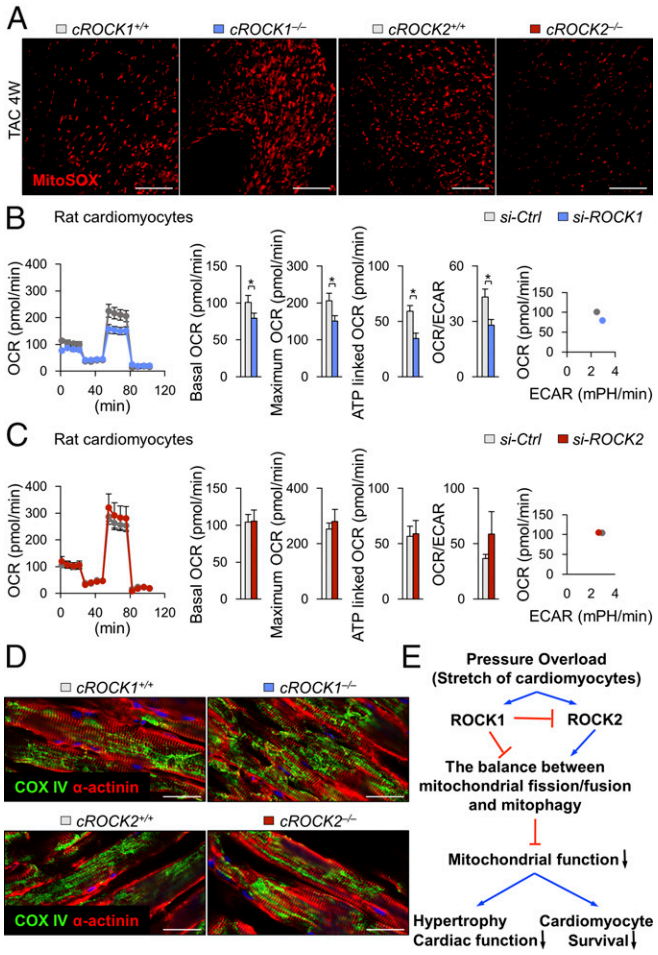

Fig. 4. Conflicting roles of ROCK1 and ROCK2 in mitochondrial function. (*A*) Representative pictures of MitoSOX staining of the LV after TAC. (Scale bars, 100 μm.) (*B*) Quantification of the mitochondrial OCR and ECAR of NRCMs after transfection with ROCK1 siRNA (*si-ROCK1*) or control siRNA (*si-Ctrl*) (n = 6 each). Bar graphs show basal OCR, maximum OCR, ATP-linked OCR, and the ratio of OCR to ECAR. (*C*) Quantification of the mitochondrial OCR and ECAR of NRCMs after transfection with ROCK2 siRNA (*si-ROCK2*) or *si-Ctrl* (n = 6 each). (*D*) Representative double immunostaining for α-actinin and COX IV (mitochondria) of the LV after TAC. (Scale bars, 25 μm.) (*E*) Schematic representation of opposing roles of ROCK1 and ROCK2 in mitochondrial function. Data represent the mean ± SEM; *$P < 0.05$. Comparisons of parameters were performed with an unpaired Student's t test.

(*Fis1*, *Mff*) in *cROCK1*$^{-/-}$ and *cROCK2*$^{-/-}$ hearts. However, the expression pattern of these genes did not change significantly in *cROCK1*$^{-/-}$ or *cROCK2*$^{-/-}$ hearts compared with their respective controls under pressure overload (*SI Appendix*, Fig. S10 *C* and *D*). Here, we examined the expressions of genes associated with mitochondrial fusion (*Mfn1*, *Mfn2*, and *Opa1*) in *cROCK1*$^{-/-}$ and *cROCK2*$^{-/-}$ hearts. Notably, the expressions of fusion genes were significantly lower in *cROCK1*$^{-/-}$ hearts than in *cROCK1*$^{+/+}$ hearts under pressure overload (*SI Appendix*, Fig. S10*E*). In contrast, the expression of fusion genes did not significantly change or slightly increased in *cROCK2*$^{-/-}$ hearts compared with *cROCK2*$^{+/+}$ hearts under pressure overload (*SI Appendix*, Fig. S10*F*). We further examined the expressions of genes related to mitophagy (*Pink1* and *Park2*) in *cROCK1*$^{-/-}$ and *cROCK2*$^{-/-}$ hearts. Notably, *Pink1* expression was significantly lower in *cROCK1*$^{-/-}$ hearts than in *cROCK1*$^{+/+}$ hearts under pressure overload (*SI Appendix*, Fig. S10*G*). In contrast, *Pink1* expression did not change in *cROCK2*$^{-/-}$ hearts compared with *cROCK2*$^{+/+}$ hearts (*SI Appendix*, Fig. S10*H*). Finally, *Park2* expression was significantly lower in both *cROCK1*$^{-/-}$ and *cROCK2*$^{-/-}$ hearts compared with their respective controls at baseline and under pressure overload (*SI Appendix*, Fig. S10 *G* and *H*).

Next, using a Seahorse XF24-3 apparatus, which provides information on mitochondrial function through real-time measurements of oxygen consumption rate (OCR; a marker of oxidative phosphorylation) and extracellular acidification rate (ECAR; a surrogate marker for glycolysis), we examined ROCK-mediated responses in NRCMs after ROCK silencing by siRNA (Fig. 4 *B* and *C*). OCR reflects the mitochondrial respiration rate and energy production and ECAR reflects the rate of glycolysis in NRCMs. Silencing of ROCK1 by siRNA significantly decreased the OCR/ECAR ratio and maximal OCR compared with the control siRNA (Fig. 4*B*). In contrast, silencing of ROCK2 by siRNA increased the OCR/ECAR ratio and maximal OCR compared with the control siRNA (Fig. 4*C*), suggesting opposite roles for ROCK1 and ROCK2 in mitochondrial function. There is mounting evidence that mitochondrial dynamics are relevant to the mechanisms of apoptosis, cell proliferation, and mitochondrial energy metabolism in HF (31). *cROCK1*$^{-/-}$ hearts showed reduced expressions of genes associated with mitochondrial fusion (*Mfn1*, *Mfn2*, and *Opa1*) and mitophagy (*Pink1*), promoting impaired mitochondrial fusion and fragmentation of the mitochondrial networks. Consistently, *cROCK1*$^{-/-}$ hearts showed significantly increased phosphorylation of Drp1 (S616) and significantly reduced Drp1 (S637) under pressure overload than *cROCK1*$^{+/+}$ hearts (*SI Appendix*, Fig. S11*A*). In contrast, Drp1 phosphorylation did not differ between *cROCK2*$^{+/+}$ and *cROCK2*$^{-/-}$ hearts both at baseline and under pressure overload (*SI Appendix*, Fig. S11*B*). Thus, we next examined the morphology of mitochondria in *cROCK1*$^{-/-}$ and *cROCK2*$^{-/-}$ hearts. Consistent with the mitochondrial gene expressions, *cROCK1*$^{-/-}$ hearts showed a more fragmented mitochondrial morphology than *cROCK1*$^{+/+}$ hearts (Fig. 4*D*), which was further confirmed by transmission electron microscopy (*SI Appendix*, Fig. S11*C*). In contrast, *cROCK2*$^{-/-}$ hearts showed a less fragmented mitochondrial morphology than *cROCK2*$^{+/+}$ hearts (Fig. 4*D*). These results suggest that the balance between mitochondrial fission/fusion and mitophagy is fundamentally regulated by ROCK1 and ROCK2 in cardiomyocytes. Additionally, ROCK1 and ROCK2 regulate the switch from oxidative phosphorylation to anaerobic metabolism as an adaptive response to mitochondrial dysfunction, especially under pressure overload (Fig. 4*E*).

ROCK1 and ROCK2 in Cardiomyocytes for Postcapillary PH and Survival. As CyPA and Bsg are known to exacerbate cardiac hypertrophy and pulmonary vascular remodeling through augmentation of oxidative stress (29, 32, 33), we next examined their expressions in hearts and lungs. Myocardial expressions of CyPA and Bsg were up-regulated in *cROCK1*$^{-/-}$ hearts (*SI Appendix*, Figs. S12 and S13*A*), whereas myocardial expression of CyPA was down-regulated in *cROCK2*$^{-/-}$ hearts (*SI Appendix*, Figs. S12 and S13*B*). Additionally, protein levels of CyPA and Bsg, both of which promote proliferation of pulmonary artery smooth muscle cells (PASMCs) and the development of PH (33), were significantly increased in lungs from *cROCK1*$^{-/-}$ mice compared with lungs from *cROCK1*$^{+/+}$ mice after TAC (*SI Appendix*, Fig. S13*C*), whereas the levels of CyPA were significantly lower in lungs from *cROCK2*$^{-/-}$ mice than in lungs from *cROCK2*$^{+/+}$ mice after TAC (*SI Appendix*, Fig. S13*D*). These results suggest that ROCK1 and ROCK2 in cardiomyocytes affect CyPA/Bsg-mediated ROS production in the heart and lung after pressure overload (*SI Appendix*, Fig. S13*E*).

It was previously demonstrated that endothelial permeability in pulmonary circulation is increased in patients with postcapillary PH (34). Consistently, the increase in lung weight ratio was significantly higher in *cROCK1*$^{-/-}$ mice than in *cROCK1*$^{+/+}$ mice

after TAC (Fig. 5*A*). Furthermore, as elevated filling pressures by pressure overload are enhanced by ROCK1 deficiency but attenuated by ROCK2 deficiency (*SI Appendix*, Fig. S3), we next examined pulmonary vascular remodeling, which indicates the development of postcapillary PH. Histological analysis of the lung showed an increased medial thickness and muscularization of distal pulmonary arteries in *cROCK1*$^{-/-}$ mice compared with *cROCK2*$^{-/-}$ mice under pressure overload (Fig. 5*B*). Consistent with the morphological changes, *cROCK1*$^{-/-}$ mice exhibited increased right ventricular systolic pressure (RVSP) compared with *cROCK2*$^{-/-}$ mice after TAC (Fig. 5*C*). These results indicate that ROCK1 protect against the development of postcapillary PH, whereas ROCK2 promotes it. Next, we performed severe TAC to confirm the survival of *cROCK1*$^{-/-}$ mice compared with *cROCK2*$^{-/-}$ mice. Importantly, *cROCK1*$^{-/-}$ mice showed a significantly poor survival rate compared with *cROCK2*$^{-/-}$ mice after severe TAC (Fig. 5*D*). Consistently, the extents of TAC-induced LV dilatation and reduced contractility were significantly higher in *cROCK1*$^{-/-}$ mice than in *cROCK2*$^{-/-}$ mice (Fig. 5*E*). These results indicate that ROCK1 protects the heart from hypertrophy, fibrosis, and reduced contractility, resulting in postcapillary PH, whereas ROCK2 deteriorate them under severe pressure overload (Fig. 5*F*). Postcapillary PH increases right ventricular pressure overload and secondarily induces hypoxia and systemic inflammation, promoting HF and death (7, 9). Thus, targets that belong to both the mechanisms underlying both HF and postcapillary PH may represent novel therapeutic targets (Fig. 5*F*).

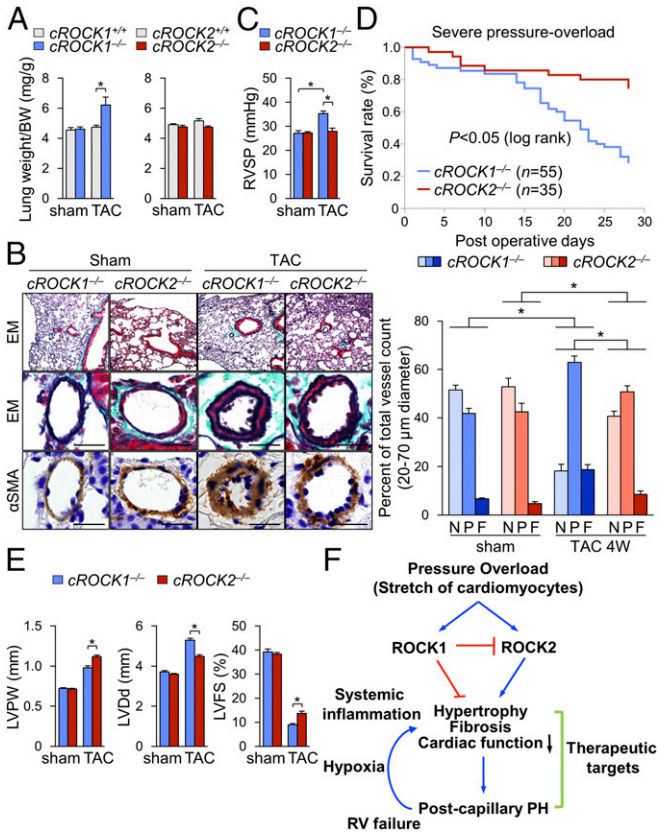

Fig. 5. ROCK1 and ROCK2 in cardiomyocytes for postcapillary PH and survival. (*A*) The ratio of lung weight to body weight (BW) in *cROCK1*$^{+/+}$, *cROCK1*$^{-/-}$, *cROCK2*$^{+/+}$, and *cROCK2*$^{-/-}$ mice at 4 wk after TAC (n = 12 each) or sham operation (n = 5 each). (*B*, *Left*) Representative EM and immunostaining for α-smooth muscle actin (αSMA) of the distal pulmonary arteries (PA) in *cROCK1*$^{-/-}$ and *cROCK2*$^{-/-}$ mice at 4 wk after TAC or sham operation. (Scale bars, 25 μm.) (*B*, *Right*) Muscularization ratios of distal PAs in *cROCK1*$^{-/-}$ and *cROCK2*$^{-/-}$ mice at 4 wk after TAC (n = 10 each) or sham operation (n = 5 each). F, fully muscularized vessels; N, nonmuscularized vessels; P, partially muscularized vessels. (*C*) RVSP in *cROCK1*$^{-/-}$ and *cROCK2*$^{-/-}$ mice at 4 wk after TAC (n = 6 each) or sham operation (n = 6 each). (*D*) Survival rates of *cROCK1*$^{-/-}$ (n = 55) and *cROCK2*$^{-/-}$ mice (n = 35) subjected to severe TAC. Results are expressed as log-rank test. (*E*) Quantitative analysis of the parameters of cardiac function assessed by echocardiography in *cROCK1*$^{-/-}$ and *cROCK2*$^{-/-}$ mice at 4 wk after severe TAC (n = 12 each) or sham operation (n = 5 each). (*F*) Schematic representation of the different roles of ROCK1 and ROCK2 in cardiomyocytes for the development of postcapillary PH and survival. Data represent the mean ± SEM; *P < 0.05. Comparisons of parameters were performed with two-way ANOVA followed by Tukey's honestly significant difference test for multiple comparisons.

Celastrol Attenuates Cardiac Dysfunction and Postcapillary PH. In the present study, pressure overload up-regulated CyPA and Bsg in the heart and lung from *cROCK1*$^{-/-}$ mice compared with the respective controls, whereas the heart and lung from *cROCK2*$^{-/-}$ mice showed significantly lower protein levels of CyPA. We have demonstrated that CyPA and Bsg, which augment oxidative stress, promote the development of HF (29, 32) and PH (33). Importantly, plasma levels of soluble Bsg (sBsg) are increased in HF patients (29). Moreover, patients with higher sBsg present with poor prognosis. In the present study, plasma levels of CyPA were significantly increased in HF patients and were higher in patients with postcapillary PH compared with those without it (Fig. 6*A* and *SI Appendix*, Table S3). Importantly, plasma levels of CyPA were higher especially in patients with stenotic valvular disease, such as AS, mitral valve stenosis, and pulmonary valve stenosis, which were higher in patients with postcapillary PH compared with those without it (Fig. 6*A*). Moreover, patients with higher CyPA levels showed poor prognosis during the 5.5-y follow-up period (Fig. 6 *B* and *C*).

Based on the experimental findings and previous reports regarding the crucial role of CyPA and Bsg in cardiac hypertrophy and pulmonary vascular remodeling, we aimed to identify a therapeutic agent that down-regulates both CyPA and Bsg, to be used as a therapeutic agent for left heart diseases by targeting both cardiac dysfunction and postcapillary PH. To this end, we performed in silico screening with the Life Science Knowledge Bank software (www.lskb.w-fusionus.com/); however, no compound showed an inhibitory effect on both CyPA and Bsg. We then used the public chemical library in the Drug Discovery Initiative (DDI) (www.ddi.u-tokyo.ac.jp/en/), a collection of 3,336 clinically used compounds and derivatives. Since pulmonary vascular remodeling in postcapillary PH accompanies excessive proliferation of PASMCs (8), we used PASMCs from patients with pulmonary arterial hypertension (*SI Appendix*, Fig. S14*A*). We performed a high-throughput screening and identified celastrol that reduced the expressions of both CyPA (*PPIA*) and Bsg (*BSG*) as well as proliferation of PASMCs (Fig. 6*D*). Additionally, celastrol treatment suppressed CyPA and Bsg expression in NRCMs (Fig. 6*E*). Celastrol has antioxidant, antiinflammatory, and antiproliferative properties (35). We then examined the effect of celastrol in TAC-induced HF in mice (Fig. 6*F*). Importantly, TAC-induced increases in CyPA and Bsg in the heart and lung were significantly attenuated by celastrol treatment compared with vehicle controls (*SI Appendix*, Fig. S14 *B* and *C*). Interestingly, ROCK2 expression was suppressed while ROCK1 expression was unaffected by celastrol treatment compared with vehicle controls in the heart after TAC (*SI Appendix*, Fig. S14*C*). Consistently, celastrol significantly reduced the increase in heart weight/body weight after TAC compared with vehicle controls (Fig. 6*G*). Moreover, celastrol significantly ameliorated TAC-induced increases in RVSP (Fig. 6*H*) and cardiac dysfunction assessed by echocardiography (Fig. 6*I*) compared with vehicle controls. Further histological analysis showed that celastrol treatment attenuated pressure-overload-induced cardiac hypertrophy and fibrosis compared with vehicle controls

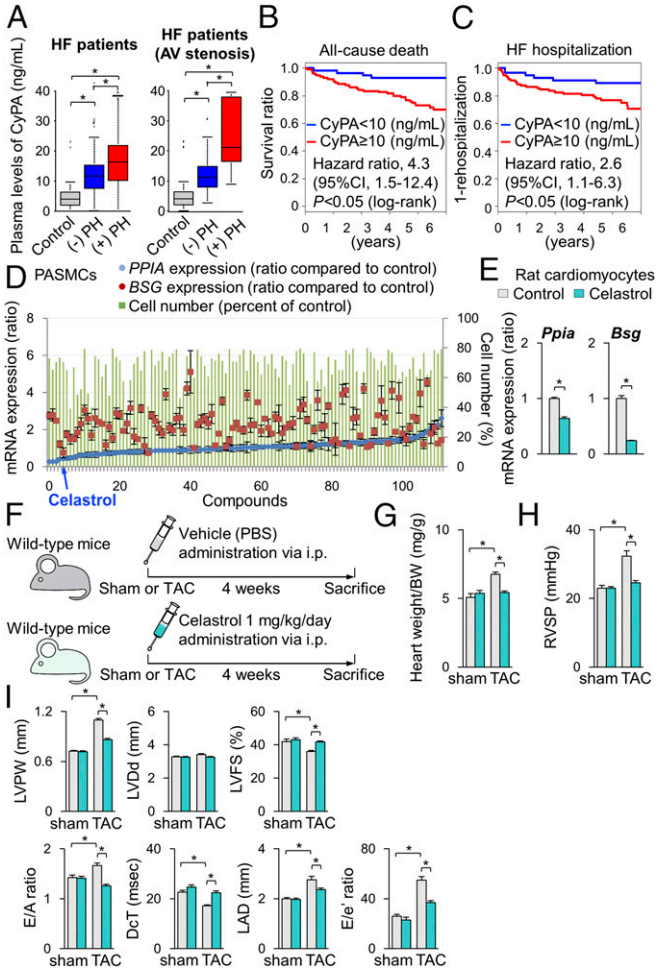

Fig. 6. Celastrol ameliorates cardiac dysfunction and postcapillary PH. (*A*, *Left*) Plasma levels of cyclophilin A (CyPA) in patients with HF with ($n = 54$) or without ($n = 72$) postcapillary PH compared with controls ($n = 25$). (*B*, *Right*) Plasma levels of CyPA in patients with stenotic valvular disease, such as AS, mitral valve stenosis, and pulmonary valve stenosis with ($n = 18$) or without ($n = 27$) postcapillary PH compared with controls ($n = 25$). (*B* and *C*) Kaplan–Meier curve in patients with HF. Higher plasma CyPA levels (≥10 ng/mL) were significantly associated with (*B*) all-cause death and (*C*) HF hospitalization, compared with lower plasma CyPA levels (<10 ng/mL). (*D*) Results of the 113 compounds that suppress PASMC proliferation (green bars) and *Ppia* (CyPA, blue plots) and *Bsg* (Bsg, red plots) gene expression. (*E*) Relative mRNA expressions of *Ppia* and *Bsg* in NRCMs after treatment with celastrol or vehicle for 24 h ($n = 3$ each). (*F*) Schematic protocols for celastrol administration to wild-type mice subjected to TAC or sham operation, in which celastrol (1 mg/kg/d) or control vehicle was administered by i.p. injection. (*G*) The ratio of heart weight/body weight (BW) after treatment with celastrol or control vehicle for 4 wk (TAC, $n = 15$ each; sham $n = 5$ each). (*H*) RVSP after treatment with celastrol or vehicle for 4 wk (TAC, $n = 15$ each; sham $n = 5$ each). (*I*) Quantitative analysis of the echocardiographic parameters of cardiac function after treatment with celastrol or control vehicle for 4 wk (TAC, $n = 15$ each; sham $n = 5$ each). Data represent the mean ± SEM; $^*P < 0.05$. Comparisons of parameters were performed with two-way ANOVA followed by Tukey's honestly significant difference test for multiple comparisons.

(*SI Appendix*, Fig. S15 *A* and *B*). Finally, we examined the effect of celastrol on TAC-induced HF in *cROCK1*$^{-/-}$ mice (*SI Appendix*, Fig. S16*A*). Celastrol significantly ameliorated pressure-overload-induced cardiac dysfunction and postcapillary PH in *cROCK1*$^{-/-}$ mice (*SI Appendix*, Fig. S16 *B–D*). These results suggest that celastrol suppresses the expression of CyPA and Bsg in the heart and lung, thereby ameliorating both HF and postcapillary PH in mice.

Discussion

Contrasting Roles of Myocardial ROCK1 and ROCK2 in Response to Pressure Overload. Although ROCK1 and ROCK2 are highly homologous, sharing 65% homology in their amino acid sequence and 92% homology in their kinase domain (21), functional differences between the two isoforms remain to be fully elucidated, especially in cardiomyocytes. This study demonstrates the different roles of ROCK1 and ROCK2 in cardiomyocytes in response to pressure overload. Interestingly, *cROCK1*$^{-/-}$ mice were vulnerable to pressure overload associated with enhanced cardiac hypertrophy and fibrosis, suggesting that ROCK1 in cardiomyocytes protects the heart against pressure overload. Indeed, cleaved ROCK1 is increased in the human failing heart, which induces apoptosis in cardiomyocytes (36). Thus, adequate activity of ROCK1 in cardiomyocytes is essential to maintain cardiac functions in loaded conditions, suggesting that inhibition of ROCK1 is not a suitable therapeutic strategy for HF. Identification of substrates of myocardial ROCK1 should provide further insights into the specific roles of ROCK1 in cardiomyocytes. Surprisingly, there is a report showing that systemic *ROCK1*$^{-/-}$ mice presented with reduced cardiac fibrosis in response to pressure overload (23). Different phenotypes between the systemic *ROCK1*$^{-/-}$ mice and our cardiac-specific *ROCK1*$^{-/-}$ mice under pressure overload can be explained by the different roles of ROCK1 in cardiomyocytes and other cell types (e.g., endothelial cells, vascular smooth muscle cells, and cardiac fibroblasts). Further analyses using tissue-specific ROCK1-deficient mice in inflammatory cells and cardiac fibroblasts may clarify the role of ROCK1 in cardiac fibrosis. In contrast, *cROCK2*$^{-/-}$ mice showed resistance to pressure overload with less cardiac hypertrophy in the present study. This is consistent with the previous reports indicating that myocardial ROCK2 promotes the development of angiotensin II (AngII)-induced cardiac hypertrophy (22). Moreover, a recent study demonstrated that cardiac fibroblasts-specific ROCK2 deficiency protects the heart against the development of AngII-induced cardiac hypertrophy and fibrosis (37). Thus, selective ROCK2 inhibition may be a suitable therapeutic strategy for HFpEF, which is characterized by enhanced cardiac hypertrophy and fibrosis.

Different Roles of ROCK1 and ROCK2 in ROS Production in Cardiomyocytes. We and others previously demonstrated that the Rho-kinase pathway is substantially involved in cardiac hypertrophy and failure associated with oxidative stress (17, 29, 38, 39). However, the different roles of ROCK1 and ROCK2 in ROS production in cardiomyocytes remain unclear. Mitochondria, which are continuously joined by the process of fusion and divided by the process of fission, are the major source of ROS (40). The mitochondrial network is fragmented in cardiomyocytes from HF patients (41), and this disruption is mechanistically related to impaired function of the heart. Fragmentation of the mitochondrial network reflects, in part, increased fission in cardiomyocytes (42). Fission creates smaller, more discrete mitochondria, which are more capable of generating ROS, facilitating mitophagy, and accelerating hypertrophy in cardiomyocytes (43). When mitochondria cannot divide, protein recycling does not proceed and cardiomyocytes are arrested with imbalanced metabolism, leading to reduced ATP production (31). Thus, it is conceivable that ROCK1 deficiency in cardiomyocytes destroyed the balance between fission and fusion in cardiomyocytes, resulting in reduced mitochondrial network and increased cardiac hypertrophy, apoptosis, and fibrosis. ROCK1-mediated alteration in this balance may be modulated by the up-regulation of NOX4, which is excessively activated in the heart in response to pressure overload and is likely an upstream regulator for impaired mitochondrial fusion and enhanced fission in loaded cardiomyocytes (40). Here,

we found significantly higher levels of mitochondrial ROS in the heart of *cROCK1*$^{-/-}$ mice. As ROCK1 directly phosphorylates Drp1 and regulates the balance of mitochondrial fission/fusion in endothelial cells (26), lack of ROCK1 in cardiomyocytes may lead to impaired mitochondrial homeostasis and subsequent ROS generation. Furthermore, we previously showed the colocalization of ROS and ROCK2 expression in the heart after pressure overload (17). Thus, substantial compensatory up-regulation of ROCK2 in the heart from *cROCK1*$^{-/-}$ mice may reflect increased levels of ROS after pressure overload, indicating that ROCK2 specifically augments ROS production in the failing heart. Consistently, the amount of ROS was significantly reduced in the heart from *cROCK2*$^{-/-}$ mice after pressure overload.

In a previous study, we demonstrated that treatment with fasudil, a specific Rho-kinase inhibitor, reduced the levels of ROS in the heart in animal models of HF (19). Thus, the present study indicates that fasudil-mediated reduction in ROS is associated with the inhibition of ROCK2 in cardiomyocytes. However, further mechanistic studies are needed to elucidate the different roles of ROCK1 and ROCK2 in ROS production in cardiomyocytes in response to pressure overload. Interestingly, CyPA and Bsg play critical roles as downstream targets of Rho-kinase in the enhancement of ROS production. CyPA is one of the causative proteins that mediate oxidative stress-induced cardiovascular dysfunctions, such as atherosclerosis, abdominal aortic aneurysm, and cardiac hypertrophy (32, 44, 45). Furthermore, one of the CyPA receptors, Bsg, also plays crucial roles in the pathogenesis of PH, cardiac hypertrophy, and HF (29, 33). Our recent study demonstrated a synergy between Rho-kinase and CyPA to increase ROS generation (46). As ROS stimulates myocardial hypertrophy, matrix remodeling, and cellular dysfunction (47), Rho-kinase (especially ROCK2) and CyPA promote ROS production as well as cardiac hypertrophy and failure in a synergistic manner. Consistent with our recent studies, we detected a synergy between Rho-kinase, CyPA, and Bsg to increase ROS production. Thus, Rho-kinase, especially ROCK2, and CyPA may promote ROS production as well as cardiac hypertrophy and failure in a synergistic manner in the heart of *cROCK1*$^{-/-}$ mice after pressure overload. In addition, CyPA and Bsg were also up-regulated in the lung from *cROCK1*$^{-/-}$ mice after pressure overload, in which vascular remodeling and postcapillary PH were significantly developed. Both CyPA and Bsg are known to accelerate PH by stimulating oxidative stress and inflammation (33, 48). Similarly, CyPA and Bsg in the lung may also contribute to the development of postcapillary PH, which is primarily caused by the passive backward transmission of elevated filling pressure induced by LV dysfunction. Further analyses using CyPA- and Bsg-deficient mice may reveal the specific roles of CyPA and Bsg in pressure-overload-induced cardiac dysfunction and postcapillary PH. Taken together, our findings indicate that inhibiting both CyPA and Bsg may represent a novel therapeutic strategy for the treatment of HF patients with postcapillary PH. As patients with HF and coexisting postcapillary PH show poor clinical outcomes (7, 9), targeting both cardiac dysfunction and pulmonary vascular remodeling could be a novel concept for the treatment of HF.

Celastrol as a Novel Therapeutic Agent for HF Patients with Postcapillary PH. We demonstrated that fasudil, a specific inhibitor of both ROCK1 and ROCK2, is effective in animal models of HF (19, 38). In contrast, we previously demonstrated that Rho-kinase inhibition in mice by SM22α promoter-driven overexpression of dominant-negative Rho-kinase showed arrhythmogenic right ventricular cardiomyopathy (49). This result indicates that long-term isoform nonselective inhibition of Rho-kinase may have an impact on cardiac function. Indeed, in the present study, we showed that pressure-overload-induced cardiac dysfunction and postcapillary PH were accelerated in *cROCK1*$^{-/-}$ mice compared with littermate controls, suggesting that ROCK1 plays crucial role to maintain cardiac function in loaded conditions. In contrast, *cROCK2*$^{-/-}$ mice showed decreased cardiac hypertrophy compared with littermate controls after TAC. Furthermore, ROCK2 in cardiac fibroblasts is necessary to cause cardiac hypertrophy and fibrosis (37). It has recently been demonstrated that a selective ROCK2 inhibitor, KD025, could be an effective treatment for ischemic stroke and autoimmune diseases (50, 51). The present study indicates that selective ROCK2 inhibition could be a more favorable therapy for HF.

However, in the present study, cardiomyocyte-specific ROCK2-deficient mice showed a slight, but not dramatic, improvement in cardiac hypertrophy and fibrosis under pressure overload. Moreover, when we consider the complex interactions between ROCK1 and ROCK2 in cardiomyocytes and other cell types, the use of selective ROCK2 inhibitor may not meet the clinical needs to cure patients with HFpEF. Here, we also consider that HF patients with postcapillary PH show worse exercise tolerance and poor prognosis (7, 9). Thus, we decided to target both HF and postcapillary PH. To this end, we focused on CyPA and Bsg as common molecules that augment HF and PH. Here, we used PASMCs and high-throughput screening to identify novel agents to inhibit both CyPA and Bsg. In the present study, we aimed to develop a novel therapeutic agent by focusing on both CyPA and Bsg, two downstream targets of Rho-kinase (13). As an additional strategy for HF with postcapillary PH, effective treatment that achieves inhibition or reverses remodeling of pulmonary arteries is warranted (34). PASMCs in the remodeled pulmonary arteries have special characteristics with proproliferative features. Based on the development of academic drug discovery, we focused on the inhibition of PASMC proliferation to discover a novel drug for HF with postcapillary PH. The DDI was founded in Japan to promote an environment in which academic drug discovery can be performed. Using these platforms, we performed drug discovery based on a clinical perspective and the knowledge of the pathogenesis of HF. In the present study, we performed phenotypic screening and discovered compounds with inhibitory effects on CyPA and Bsg. We finally selected celastrol, presenting with antioxidant effects, for in vivo treatment. Celastrol improved pressure-overload-induced cardiac dysfunction and postcapillary PH with no apparent side effects. Thus, celastrol may be a promising drug for HF. Celastrol is a compound obtained from *Tripterygium wilfordii* and its usefulness has been reported in some inflammatory diseases, such as rheumatoid arthritis, systemic lupus erythematosus, inflammatory bowel diseases, osteoarthritis, and allergy (35). Celastrol suppresses the activity of NF-κB, which up-regulates inflammatory genes and enhances cardiac hypertrophy (52) and pulmonary vascular remodeling (53). As CyPA and Bsg activate NF-κB (48, 54), the effect of celastrol on HF may have been due to the inhibition of CyPA/Bsg-NF-κB axis, which enhances ROS generation and inflammatory status. However, the beneficial effects of celastrol may involve mechanisms other than reducing CyPA and Bsg. Further analyses are required to identify the molecular and cellular targets of celastrol in the treatment of HF.

Materials and Methods

To generate cardiac-specific ROCK1-deficient (*cROCK1*$^{-/-}$) mice and cardiac-specific ROCK2-deficient (*cROCK2*$^{-/-}$) mice, *Rock1*$^{flox/flox}$ mice and *Rock2*$^{flox/flox}$ mice were crossed with *Myh6-cre*$^{+/-}$ mice. The offspring were intercrossed. The resulting offspring, *Rock1*$^{flox/flox}$/*Myh6-cre*$^{+/-}$ mice (*cROCK1*$^{-/-}$ mice), *Rock2*$^{flox/flox}$/*Myh6-cre*$^{+/-}$ mice (*cROCK2*$^{-/-}$ mice), and their littermates were used for experiments. Additional materials and procedures can be found in *SI Appendix, Supplementary Methods*.

All animal experiments were conducted in accordance with the protocols approved by the Tohoku University Animal Care and Use Committee (no. 2017-Kodo-004).

ACKNOWLEDGMENTS. We thank the laboratory members in the Department of Cardiovascular Medicine of Tohoku University Graduate School of Medicine for valuable technical assistance, especially Hiromi Yamashita, Ai Nishihara, and Yumi Watanabe.

1. Roger VL (2013) Epidemiology of heart failure. *Circ Res* 113:646–659.
2. Paulus WJ, van Ballegoij JJ (2010) Treatment of heart failure with normal ejection fraction: An inconvenient truth! *J Am Coll Cardiol* 55:526–537.
3. Holland DJ, Kumbhani DJ, Ahmed SH, Marwick TH (2011) Effects of treatment on exercise tolerance, cardiac function, and mortality in heart failure with preserved ejection fraction. A meta-analysis. *J Am Coll Cardiol* 57:1676–1686.
4. Loffredo FS, Nikolova AP, Pancoast JR, Lee RT (2014) Heart failure with preserved ejection fraction: Molecular pathways of the aging myocardium. *Circ Res* 115:97–107.
5. Redfield MM (2004) Understanding "diastolic" heart failure. *N Engl J Med* 350: 1930–1931.
6. Hill JA, Olson EN (2008) Cardiac plasticity. *N Engl J Med* 358:1370–1380.
7. Vachiéry JL, et al. (2013) Pulmonary hypertension due to left heart diseases. *J Am Coll Cardiol* 62(Suppl):D100–D108.
8. Delgado JF, et al. (2005) Pulmonary vascular remodeling in pulmonary hypertension due to chronic heart failure. *Eur J Heart Fail* 7:1011–1016.
9. Ghio S, et al. (2001) Independent and additive prognostic value of right ventricular systolic function and pulmonary artery pressure in patients with chronic heart failure. *J Am Coll Cardiol* 37:183–188.
10. Lai YC, et al. (2016) SIRT3-AMP-activated protein kinase activation by nitrite and metformin improves hyperglycemia and normalizes pulmonary hypertension associated with heart failure with preserved ejection fraction. *Circulation* 133:717–731.
11. Aguero J, et al. (2016) Intratracheal gene delivery of SERCA2a ameliorates chronic post-capillary pulmonary hypertension: A large animal model. *J Am Coll Cardiol* 67: 2032–2046.
12. Shimokawa H, Satoh K (2015) 2015 ATVB plenary lecture: Translational research on rho-kinase in cardiovascular medicine. *Arterioscler Thromb Vasc Biol* 35:1756–1769.
13. Shimokawa H, Sunamura S, Satoh K (2016) RhoA/Rho-kinase in the cardiovascular system. *Circ Res* 118:352–366.
14. Kandabashi T, et al. (2000) Inhibition of myosin phosphatase by upregulated rho-kinase plays a key role for coronary artery spasm in a porcine model with interleukin-1β. *Circulation* 101:1319–1323.
15. Uehata M, et al. (1997) Calcium sensitization of smooth muscle mediated by a Rho-associated protein kinase in hypertension. *Nature* 389:990–994.
16. Shimizu T, et al. (2013) Crucial role of ROCK2 in vascular smooth muscle cells for hypoxia-induced pulmonary hypertension in mice. *Arterioscler Thromb Vasc Biol* 33: 2780–2791.
17. Ikeda S, et al. (2014) Crucial role of rho-kinase in pressure overload-induced right ventricular hypertrophy and dysfunction in mice. *Arterioscler Thromb Vasc Biol* 34: 1260–1271.
18. Masumoto A, et al. (2002) Suppression of coronary artery spasm by the Rho-kinase inhibitor fasudil in patients with vasospastic angina. *Circulation* 105:1545–1547.
19. Fukui S, et al. (2008) Long-term inhibition of Rho-kinase ameliorates diastolic heart failure in hypertensive rats. *J Cardiovasc Pharmacol* 51:317–326.
20. Fukumoto Y, et al. (2013) Double-blind, placebo-controlled clinical trial with a rho-kinase inhibitor in pulmonary arterial hypertension. *Circ J* 77:2619–2625.
21. Shimizu T, Liao JK (2016) Rho-kinases and cardiac remodeling. *Circ J* 80:1491–1498.
22. Okamoto R, et al. (2013) FHL2 prevents cardiac hypertrophy in mice with cardiac-specific deletion of ROCK2. *FASEB J* 27:1439–1449.
23. Zhang YM, et al. (2006) Targeted deletion of ROCK1 protects the heart against pressure overload by inhibiting reactive fibrosis. *FASEB J* 20:916–925.
24. Vahebi S, Kobayashi T, Warren CM, de Tombe PP, Solaro RJ (2005) Functional effects of rho-kinase-dependent phosphorylation of specific sites on cardiac troponin. *Circ Res* 96:740–747.
25. Yura Y, et al. (2016) Focused proteomics revealed a novel Rho-kinase signaling pathway in the heart. *Cell Struct Funct* 41:105–120.
26. Wang W, et al. (2012) Mitochondrial fission triggered by hyperglycemia is mediated by ROCK1 activation in podocytes and endothelial cells. *Cell Metab* 15:186–200.
27. Luo M, Anderson ME (2013) Mechanisms of altered Ca^{2+} handling in heart failure. *Circ Res* 113:690–708.
28. Miura M, et al. (2010) Effect of nonuniform muscle contraction on sustainability and frequency of triggered arrhythmias in rat cardiac muscle. *Circulation* 121:2711–2717.
29. Suzuki K, et al. (2016) Basigin promotes cardiac fibrosis and failure in response to chronic pressure overload in mice. *Arterioscler Thromb Vasc Biol* 36:636–646.
30. Nickel AG, et al. (2015) Reversal of mitochondrial transhydrogenase causes oxidative stress in heart failure. *Cell Metab* 22:472–484.
31. Ikeda Y, et al. (2015) Endogenous Drp1 mediates mitochondrial autophagy and protects the heart against energy stress. *Circ Res* 116:264–278.
32. Satoh K, et al. (2011) Cyclophilin A promotes cardiac hypertrophy in apolipoprotein E-deficient mice. *Arterioscler Thromb Vasc Biol* 31:1116–1123.
33. Satoh K, et al. (2014) Basigin mediates pulmonary hypertension by promoting inflammation and vascular smooth muscle cell proliferation. *Circ Res* 115:738–750.
34. Guazzi M, Borlaug BA (2012) Pulmonary hypertension due to left heart disease. *Circulation* 126:975–990.
35. Cascão R, Fonseca JE, Moita LF (2017) Celastrol: A spectrum of treatment opportunities in chronic diseases. *Front Med (Lausanne)* 4:69.
36. Chang J, et al. (2006) Activation of Rho-associated coiled-coil protein kinase 1 (ROCK-1) by caspase-3 cleavage plays an essential role in cardiac myocyte apoptosis. *Proc Natl Acad Sci USA* 103:14495–14500.
37. Shimizu T, et al. (2017) Fibroblast deletion of ROCK2 attenuates cardiac hypertrophy, fibrosis, and diastolic dysfunction. *JCI Insight* 2:e93187.
38. Higashi M, et al. (2003) Long-term inhibition of Rho-kinase suppresses angiotensin II-induced cardiovascular hypertrophy in rats in vivo: Effect on endothelial NAD(P)H oxidase system. *Circ Res* 93:767–775.
39. Tsai SH, et al. (2017) Enhanced endothelin-1/Rho-kinase signalling and coronary microvascular dysfunction in hypertensive myocardial hypertrophy. *Cardiovasc Res* 113: 1329–1337.
40. Kuroda J, et al. (2010) NADPH oxidase 4 (Nox4) is a major source of oxidative stress in the failing heart. *Proc Natl Acad Sci USA* 107:15565–15570.
41. Schaper J, et al. (1991) Impairment of the myocardial ultrastructure and changes of the cytoskeleton in dilated cardiomyopathy. *Circulation* 83:504–514.
42. Hom J, Yu T, Yoon Y, Porter G, Sheu SS (2010) Regulation of mitochondrial fission by intracellular Ca^{2+} in rat ventricular myocytes. *Biochim Biophys Acta* 1797:913–921.
43. Ikeda Y, et al. (2015) Molecular mechanisms mediating mitochondrial dynamics and mitophagy and their functional roles in the cardiovascular system. *J Mol Cell Cardiol* 78:116–122.
44. Nigro P, et al. (2011) Cyclophilin A is an inflammatory mediator that promotes atherosclerosis in apolipoprotein E-deficient mice. *J Exp Med* 208:53–66.
45. Satoh K, et al. (2009) Cyclophilin A enhances vascular oxidative stress and the development of angiotensin II-induced aortic aneurysms. *Nat Med* 15:649–656.
46. Satoh K (2015) Cyclophilin A in cardiovascular homeostasis and diseases. *Tohoku J Exp Med* 235:1–15.
47. Takimoto E, Kass DA (2007) Role of oxidative stress in cardiac hypertrophy and remodeling. *Hypertension* 49:241–248.
48. Xue C, Sowden M, Berk BC (2017) Extracellular cyclophilin A, especially acetylated, causes pulmonary hypertension by stimulating endothelial apoptosis, redox stress, and inflammation. *Arterioscler Thromb Vasc Biol* 37:1138–1146.
49. Ellawindy A, et al. (2015) Rho-kinase inhibition during early cardiac development causes arrhythmogenic right ventricular cardiomyopathy in mice. *Arterioscler Thromb Vasc Biol* 35:2172–2184.
50. Lee JH, et al. (2014) Selective ROCK2 inhibition in focal cerebral ischemia. *Ann Clin Transl Neurol* 1:2–14.
51. Zanin-Zhorov A, et al. (2014) Selective oral ROCK2 inhibitor down-regulates IL-21 and IL-17 secretion in human T cells via STAT3-dependent mechanism. *Proc Natl Acad Sci USA* 111:16814–16819.
52. Hirotani S, et al. (2002) Involvement of nuclear factor-kappaB and apoptosis signal-regulating kinase 1 in G-protein-coupled receptor agonist-induced cardiomyocyte hypertrophy. *Circulation* 105:509–515.
53. Farkas D, et al. (2014) Nuclear factor κB inhibition reduces lung vascular lumen obliteration in severe pulmonary hypertension in rats. *Am J Respir Cell Mol Biol* 51: 413–425.
54. Yuan W, Ge H, He B (2010) Pro-inflammatory activities induced by CyPA-EMMPRIN interaction in monocytes. *Atherosclerosis* 213:415–421.